Distinguishing technicolor models via $t\bar{t}$ production at polarized photon colliders

Bin Zhang and Yuanning Gao
Center for High Energy Physics, Tsinghua University, Beijing 100084, China

Yu-Ping Kuang
CCAST (World Laboratory), P.O. Box 8730, Beijing 100080, China
*and Center for High Energy Physics, Tsinghua University, Beijing 100084, China**

(Received 20 March 2003; revised manuscript received 29 October 2004; published 15 December 2004)

We study top quark pair productions at a polarized photon collider from an e^+e^- linear collider (LC) in various improved technicolor models, namely, the one-family walking technicolor model, the top-color-assisted technicolor model, and the top-color-assisted multiscale technicolor model. Recent constraint on the top-pion mass from the precision data of R_b is considered. It is shown that, considering only the statistical errors, a polarized photon collider from a 500 GeV LC with an integrated luminosity of 500 fb^{-1} is sufficient for distinguishing the three improved technicolor models experimentally.

DOI: 10.1103/PhysRevD.70.115012 PACS numbers: 12.60.Nz, 13.40.–f, 14.65.Ha

Although the standard model (SM) has successfully passed the precision electroweak tests, its electroweak symmetry breaking (EWSB) mechanism is still unclear. The Higgs boson has not been found, and the LEP2 bound on the Higgs boson mass is 114.4 GeV [1]. Furthermore, the SM Higgs sector suffers from the well-known problems of *triviality* and *unnaturalness* arising from the elementary Higgs field. There have been many new physics models of the EWSB mechanism proposed for avoiding the above problems. An attractive idea of completely avoiding triviality and unnaturalness is to abandon the elementary Higgs field(s), such as various kinds of improved technicolor models [2–4], top quark seesaw models [5], and certain little Higgs models [6]. In a previous paper [7], we studied the tests of various improved technicolor models via top quark pair productions at high energy photon colliders. Since the pseudo Goldstone bosons (PGBs) coupling to the top quark in different improved technicolor models are quite different, we showed that different improved technicolor models can be distinguished experimentally through top quark pair productions at an unpolarized photon collider built from a $\sqrt{s} = 1.5$ TeV e^+e^- linear collider (LC) [7]. In this paper, we study the same processes at polarized photon colliders and take into account the recent bound on the top-pion mass from the precision data of R_b [8]. We shall see that, considering only statistical uncertainties, a polarized photon collider built from a $\sqrt{s} = 500$ GeV LC with an integrated luminosity of 500 fb^{-1} is sufficient for distinguishing the improved technicolor models.

It has been shown that the polarization of the initial laser beam and the electron beam will significantly affect the photon spectrum at the photon collider [9]. Let P_c be the polarization of the initial laser, λ_e be the polarization of the electron in the first beam, and $\tilde{P}_c$ and $\tilde{\lambda}_e$ be the corresponding parameters in the second beam, respectively. It is shown in Ref. [9] that the colliding photons will peak in a narrow region near the high energy end (80% of the electron energy) if $2\lambda_e P_c = -1$. This improves the monochromatization and enhances the effective energy of the colliding photons at the photon collider. We shall see that this effect leads to the possibility of distinguishing different improved technicolor models at a polarized photon collider built from a $\sqrt{s} = 500$ GeV LC.

Let E_e, ω_0, ω, and $\sqrt{s}(\sqrt{\hat{s}})$ be the incident electron energy, the laser-photon energy, the backscattered photon energy, and the center-of-mass energies of e^+e^- $(\gamma\gamma)$, respectively. The photon luminosity $dL_{\gamma\gamma}$ is [10]

$$dL_{\gamma\gamma} = 2zdz \int_{z^2/x_{\max}}^{x_{\max}} \frac{dx}{x} F_{\gamma/e}(x) F_{\gamma/e}(z^2/x), \qquad (1)$$

with $z = \sqrt{\hat{s}/s}$, and $x_{\max} = \omega_{\max}/E_e$,

$$F_{\gamma/e}(x) = \frac{1}{D(\xi)}\Big[1 - x + \frac{1}{1-x} - \frac{4x}{\xi(1-x)} + \frac{4x^2}{\xi^2(1-x)^2} - 2\lambda_e P_c\Big(\frac{x}{1-x} - \frac{2x^2}{(1-x)^2\xi}\Big)(2-x)\Big],$$

and

$$D(\xi) = \Big(1 - \frac{4}{\xi} - \frac{8}{\xi^2}\Big)\ln(1+\xi) + \frac{1}{2} + \frac{8}{\xi} - \frac{1}{1(1+\xi)^2},$$

where $\xi = 4E_e\omega_0/m_e^2$. In order to avoid the creation of e^+e^- pairs by the interaction of the incident and backscattered photons, ξ should not be larger than 4.8 [9]. As in Ref. [7], we take $\xi = 4.8$, then $x_{\max} \approx 0.83$ and $D(\xi) = 1.8$. The formula for the counting rate of $\gamma\gamma \to X$ at a polarized photon collider has been given in Ref. [9]. It is

$$d\dot{N}_{\gamma\gamma\to X} = dL_{\gamma\gamma}(d\sigma + \Lambda d\tau + \zeta_2\tilde{\zeta}_2 d\tau^a + \zeta_2 d\sigma_{20} + \tilde{\zeta}_2 d\sigma_{02}), \qquad (2)$$

where ζ_i $(\tilde{\zeta}_i)$, $i = 1, 2, 3$ are Stokes parameters [9],

*Mailing address.

$$\zeta_2 = \frac{C_{20}}{C_{00}},$$
$$C_{00} = \frac{1}{1-x} + 1 - x - 4r(1-r) - 2\lambda_e P_c r\xi(2r-1)(2-x),$$
$$C_{20} = 2\lambda_e r\xi[1 + (1-x)(2r-1)^2] - P_c(2r-1)\left(\frac{1}{1-x} + 1 - x\right),$$
$$x \equiv \frac{\omega}{E_e},$$
$$r \equiv \frac{x}{\xi(1-x)},$$

σ_{ij}, $i, j = 0, 1, 2, 3$ are cross sections defined in Ref. [11], $\Lambda = \langle \zeta_3\tilde{\zeta}_3 - \zeta_1\tilde{\zeta}_1 \rangle$ [9], and $d\sigma$, $d\tau^a$ are [9]

$$\begin{aligned} d\sigma &= \tfrac{1}{4}(|M_{++}|^2 + |M_{--}|^2 + |M_{+-}|^2 + |M_{-+}|^2)d\Gamma, \\ d\tau^a &= \tfrac{1}{4}(|M_{++}|^2 + |M_{--}|^2 - |M_{+-}|^2 - |M_{-+}|^2)d\Gamma, \end{aligned} \tag{3}$$

in which the subscripts + and − indicate that the photon helicity is +1 and −1, respectively, and

$$d\Gamma = \frac{(2\pi)^4}{4k\tilde{k}}\delta\left(k + \tilde{k} - \sum_f p_f\right)\prod_f \frac{d^3p_f}{(2\pi)^3 2\epsilon_f},$$

where k, $\tilde{k}$ and p_f are four momenta of the colliding photons and the fth final state particle, respectively. After averaging over the azimuthal angles, $d\sigma_{20}$ and $d\sigma_{02}$ vanish, and $\Lambda d\tau^a$ is negligibly small. So Eq. (2) becomes

$$d\dot{N}_{\gamma\gamma\to X} = dL_{\gamma\gamma}(d\sigma + \zeta_2\tilde{\zeta}_2 d\tau^a). \tag{4}$$

The corresponding cross section $\sigma(s)$ at an LC with center-of-mass energy $\sqrt{s}$ can be obtained by further integrating Eq. (4) over the parameter z [10]

$$\sigma(s) = \int_{2m_t/\sqrt{s}}^{x_{\max}} \frac{d\dot{N}_{\gamma\gamma\to X}}{dz}\, dz. \tag{5}$$

For the detection of the final state $t\bar{t}$, we know that the dominant decay mode of the top quark is $t \to W^+ b$. The W boson will then decay into either two leptons $l^+\nu_l$ or two quarks $q\bar{q}'$. We take the hadronic mode $q\bar{q}'$ for detecting the final state signal. The branching ratio of $W \to q\bar{q}'$ is $B(W \to q\bar{q}') = 68\%$ [1]. So the signal contains six jets including two b-quark jets. To separate the six jets, we follow Ref. [12] to impose a cut on the clustering of jets. Let $\hat{y}$ be the jet-invariant masses normalized by the visible energy. The imposed cut is [12]

$$\hat{y} > \hat{y}_{\text{cut}} = 5 \times 10^{-3}. \tag{6}$$

A possible background is $\gamma\gamma \to W^+W^-Z$ with $Z \to b\bar{b}$. We know that, at $\sqrt{s} = 500$ GeV, the cross section $\sigma(\gamma\gamma \to W^+W^-Z)$ is about a factor of 2 smaller than $\sigma(\gamma\gamma \to t\bar{t})$ [13], and the branching ratio of $Z \to b\bar{b}$ is $B(Z \to b\bar{b}) = 15\%$, so that this background is smaller than the signal by an order of magnitude.

Another possible background is $\gamma\gamma \to W^+W^-$ in which the hadronization of quarks forms six jets [12]. In an e^+e^- collision, the background cross section $\sigma(e^+e^- \to W^+W^-)$ is much larger than the signal cross section $\sigma(e^+e^- \to t\bar{t})$ [13]. However, after taking the cut (6), the signal-to-background ratio can be made greater than 10 [12]. At the photon collider with $\sqrt{s} = 500$ GeV, the signal cross section $\sigma(\gamma\gamma \to t\bar{t})$ is about the same as $\sigma(e^+e^- \to t\bar{t})$, while the background cross section $\sigma(\gamma\gamma \to W^+W^-)$ is about a factor of 10 larger than $\sigma(e^+e^- \to W^+W^-)$ [13]. Hence, at the photon collider, the signal-to-background ratio after imposing the cut (6) is about 1. So we have to tag at least one b jet to suppress the background. We know that the b-tagging efficiency at LEP and at the Tevatron is around (50–60)%. We shall take 50% for the b-tagging efficiency in the following study.

Our calculation shows that the cut (6) reduces the signal cross section $\sigma(\gamma\gamma \to t\bar{t})$ by a factor of 47% in both the SM and the technicolor models for the parameter range under consideration. To be more realistic, we take into account the fact that the detector cannot detect jets in certain forward and backward zones along the beam line. As a conservative estimate, we take the polar angle (relative to the beam line) of the undetectable zones to be $\theta < 20^\circ$ and $\theta > 160^\circ$. So we require all six jets to be in the detectable region $20^\circ < \theta < 160^\circ$. Practically, b tagging is effective only in the region $30^\circ < \theta < 150^\circ$. So we further require the tagged b jet and/or $\bar{b}$ jet to be in this effective region. There can be two possible cases:

(a) Both b and $\bar{b}$ jets are in the b-tagging effective region $30^\circ < \theta < 150^\circ$, while the other four jets are in the detectable region $20^\circ < \theta < 160^\circ$. Our calculation shows that the probability of satisfying this requirement is 58.3%. In this case, it is possible to tag both the b and the $\bar{b}$ jets. Now we only need to tag one of them without specifying whether it is b or $\bar{b}$. For each one of them, the probability of not being tagged is 50%. So the probability of both of them not being tagged is 25%. Therefore our actual b-tagging efficiency in this case is 75%.

(b) One tagged b (or $\bar{b}$) jet is in the b-tagging effective region $30^\circ < \theta < 150^\circ$, and the untagged $\bar{b}$ (or b) jet is in the detectable but not b-tagging effective region $20^\circ < \theta < 30^\circ$. The other four jets are in the

detectable region $20° < \theta < 160°$. Our calculation shows that the probability of satisfying this requirement is 10%. In this case the b-tagging efficiency is 50%.

Taking into account both of these two possible cases and the W decay branching ratio $B(W \to q\bar{q}') = 68\%$, our final detection efficiency is

$$(68\%)^2 \times 47\% \times (58.3\% \times 75\% + 10\% \times 50\%) \approx 10\%. \tag{7}$$

In recent years, two of the e^+e^- linear collider projects have been actively pushed. They are the DESY TeV Energy Superconducting Linear Accelerator (TESLA) with the designed luminosity of $3.4 \times 10^{34}\ \mathrm{cm}^{-2}\,\mathrm{sec}^{-1}$ [14] corresponding to $\int_{\mathrm{yr}} \mathcal{L}dt = 340\ \mathrm{fb}^{-1}$, and the KEK Joint Linear Collider (JLC) with the designed luminosity of $(8\text{–}9) \times 10^{33}\ \mathrm{cm}^{-2}\,\mathrm{sec}^{-1}$ [12] corresponding to $\int_{\mathrm{yr}} \mathcal{L}dt = (80\text{–}90)\ \mathrm{fb}^{-1}$. As usual, we shall take an integrated luminosity of $500\ \mathrm{fb}^{-1}$ and the 10% detection efficiency to estimate the numbers of events (N_{events}) of $\gamma\gamma \to t\bar{t}$. In this paper, only statistical errors are taken into account.

In the following, we calculate the helicity amplitudes in Eq. (3) for $\gamma\gamma \to t\bar{t}$ in various improved technicolor models. As what we did in Ref. [7], for avoiding singularities arising from the very forward or very backward scatterings, we take the rapidity and transverse momentum cuts

$$|y| < 2.5, \qquad p_T > 20\ \mathrm{GeV}, \tag{8}$$

which will also increase the relative corrections.

As in Ref. [7], we study the PGB contributions to $\gamma\gamma \to t\bar{t}$ in three technicolor models, namely, model A: the one-family walking technicolor model by Appelquist and Terning [2], model B: the top-color-assisted technicolor model by Hill [3], and model C: the top-color-assisted multiscale technicolor model by Lane [4]. The PGBs in these three models are quite different. This is the main reason why the three models can be distinguished. The formulas for the PGB-$t\bar{t}$ couplings in the three models and the production amplitudes are given in Ref. [7].

Model A.—In model A, color-singlet PGBs are composed of technileptons, which do not couple to $t\bar{t}$. Thus there is no s-channel resonance contribution in this model. The relevant PGBs are the color-octet technipions containing the $\mathrm{SU}(2)_W$ singlet Π_a^0 and the $\mathrm{SU}(2)_W$ triplet Π_a^α. Their masses are in the few hundred GeV range, and their decay constant is $f_Q \approx 140$ GeV [2]. The coupling of these PGBs to the $t(b)$ quark is [2]

$$\frac{\sqrt{2}m_t}{f_Q}\Big[i\bar{t}\gamma_5 \frac{\lambda^a}{2} t\Pi_a^0 + i\bar{t}\gamma_5 \frac{\lambda^a}{2} t\Pi_a^3 + \frac{1}{\sqrt{2}}\bar{t}(1-\gamma_5) \times \frac{\lambda^a}{2} b\Pi_a^+ + \frac{1}{\sqrt{2}}\bar{b}(1+\gamma_5)\frac{\lambda^a}{2} t\Pi_a^- \Big]. \tag{9}$$

These color-octet PGBs contribute to $\gamma\gamma \to t\bar{t}$ only through radiative corrections which are small. We list, in Table I, the obtained Π_a corrections to the $\gamma\gamma \to t\bar{t}$ cross section $\Delta\sigma$, the relative correction $\Delta\sigma/\sigma_0$ (σ_0 stands for the SM cross section), the total cross section $\sigma = \sigma_0 + \Delta\sigma$, and N_{events} for an integrated luminosity of $500\ \mathrm{fb}^{-1}$ at a polarized photon collider from a 500 GeV LC with the polarization $2\lambda_e P_c = -1$ for m_{Π_a} in the range $250 < m_{\Pi_a} < 500$ GeV given in Ref. [2]. We see that the corrections $\Delta\sigma$ are negative which are mainly from the interference between the PGB amplitude and the SM amplitude. The absolute square of the PGB amplitude is not large in this model. We see from Table I that the total cross sections σ are much larger than those given in Ref. [7] due to the enhancement of the effective photon energy in the high energy region at the polarized photon collider. We see that N_{events} for an integrated luminosity of $500\ \mathrm{fb}^{-1}$ taking account of the 10% detection efficiency are $(8\text{–}9) \times 10^3$. The corresponding 95% statistical uncertainties are about 2%. Comparing with the relative corrections $\Delta\sigma/\sigma_0 \sim -(7\text{–}16)\%$ listed in Table I, we see that the Π_a correction effect can be clearly detected.

Model B.—Model B contains a technicolor sector and a top-color sector. The technicolor sector contributes only a small portion of the top quark mass, say $m_t' = \epsilon m_t$ ($\epsilon \ll 1$), while most of the top quark mass is contributed from the top-color sector, say $m_t - m_t' = (1-\epsilon)m_t$. The $b \to s\gamma$ experiment requires $\epsilon < 0.1$ [15]. In this paper, we take a typical value $\epsilon = 0.08$, i.e., $m_t' = 0.08 m_t \approx 14$ GeV as an example to do the study.

In the technicolor sector, the coupling of the color-octet technipion to the $t(b)$ quark is similar to Eq. (9) but with m_t/f_Q replaced by m_t'/f_Π [7], i.e.,

$$\frac{\sqrt{2}m_t'}{f_\Pi}\Big[i\bar{t}\gamma_5 \frac{\lambda^a}{2} t\Pi_a^0 + i\bar{t}\gamma_5 \frac{\lambda^a}{2} t\Pi_a^3 + \frac{1}{\sqrt{2}}\bar{t}(1-\gamma_5) \times \frac{\lambda^a}{2} b\Pi_a^+ + \frac{1}{\sqrt{2}}\bar{b}(1+\gamma_5)\frac{\lambda^a}{2} t\Pi_a^- \Big]. \tag{10}$$

In addition to the color-octet technipions, there are also color-singlet technipions Π^0 and Π^3, composed of techni-

TABLE I. Technipion corrections to the $\gamma\gamma \to t\bar{t}$ cross section $\Delta\sigma$, the relative correction $\Delta\sigma/\sigma_0$, the total cross section $\sigma = \sigma_0 + \Delta\sigma$, and N_{events} for an integrated luminosity of $500\ \mathrm{fb}^{-1}$ taking account of the 10% detection efficiency at a 500 GeV e^+e^- linear colliderfor with $2\lambda_e P_c = -1$ for various values of m_{Π_a} in model A (the SM cross section is $\sigma_0 = 196$ fb).

m_{Π_a} (GeV)	$\Delta\sigma$ (fb)	$\Delta\sigma/\sigma_0$ (%)	σ (fb)	N_{events}
250	−31	−15.8	165	8250
300	−26	−13.3	170	8500
350	−22	−11.2	174	8700
400	−19	−9.7	177	8850
500	−14	−7.1	182	9100

quarks, with the decay constant $f_\Pi \approx 120$ GeV, and masses in the few hundred GeV range. The coupling of these color-singlet PGBs to $t(b)$ quarks is [7]

$$\frac{c_t m_t'}{\sqrt{2} f_\Pi}\Big[i\bar{t}\gamma_5 t\Pi^0 + i\bar{t}\gamma_5 t\Pi^3 + \frac{1}{\sqrt{2}}\bar{t}(1-\gamma_5)b\Pi^+ + \frac{1}{\sqrt{2}}\bar{b}(1+\gamma_5)t\Pi^-\Big], \quad (11)$$

$$c_t = 1/\sqrt{6}.$$

In the top-color sector, there are color-singlet top pions Π_t^0 and $\Pi_t^\pm$ with the decay constant $f_{\Pi_t} \approx 50$ GeV. The coupling of the top pions to the $t(b)$ quark is [7]

$$\frac{m_t - m_t'}{\sqrt{2} f_{\Pi_t}}\Big[i\bar{t}\gamma_5 t\Pi_t^0 + \frac{1}{\sqrt{2}}\bar{t}(1-\gamma_5)b\Pi_t^+ + \frac{1}{\sqrt{2}}\bar{b}(1+\gamma_5)t\Pi_t^-\Big]. \quad (12)$$

Recently, it has been pointed out that the LEP precision data of R_b gives important constraint on the top-pion mass [8]. With $\epsilon = 0.08$, the 2σ bound from R_b on the top-pion mass in this model is roughly $300 \le m_{\Pi_t} \le 900$ GeV [8]. The naturalness of the model favors lower values of m_{Π_t}. So we take $300 \le m_{\Pi_t} \le 500$ GeV in this study. In Ref. [7], m_{Π_t} was taken to be in the range of 180–300 GeV according to the original paper, Ref. [3]. Such a range is below the recent lower bound. We shall see that the updated heavier Π_t will make the situation quite different at the polarized photon collider from the 500 GeV LC.

The color-singlet PGBs Π^0, Π^3, and Π_t^0 couple to the initial state photons through triangle fermion loops (techniquark loops and top quark loops), so they can contribute s-channel resonances in $\gamma\gamma \to t\bar{t}$. The triangle fermion loops are enhanced by the anomaly, so that the s-channel resonance contributions can be of the order of tree level contributions. These s-channel resonance contributions are dominant in models B and C. If the PGB mass is greater than $2m_t$, it can decay into $t\bar{t}$. The decay rate is determined by the PGB-$t-\bar{t}$ coupling strengths given in Eqs. (11) and (12). Since $m_t - m_t'/f_{\Pi_t}$ in Eq. (12) is large, the width of Π_t^0 will be large if its mass is greater than $2m_t$. In this case, the s-channel resonance effect from Π_t^0 is not so significant. On the other hand, m_t'/f_Π in Eq. (11) is small, so that the resonance effects from Π^0 and Π^3 are significant even if their masses are greater than $2m_t$. The width of Π^3 is very small which is hard to detect experimentally [7]. So we concentrate on examining the s-channel resonance effect of Π^0 and simply take a typical mass of $m_{\Pi^3} = 300$ GeV for Π^3.

The obtained $\Delta\sigma$, $\Delta\sigma/\sigma_0$, σ, and N_{events} for an integrated luminosity of 500 fb^{-1} taking account of the 10% detection efficiency for $m_{\Pi_t^0} = 300$ and 400 GeV, and $m_{\Pi^0} = 300$, 400, and 500 GeV in this model are listed in Table II. We see that, in the case of $m_{\Pi_t^0} = 300$ GeV, $\Delta\sigma$ is more negative than in model A because there is s-channel Π_t^0 and Π^0 resonance contributions in addition to the radiative corrections, and the s-channel resonance contributions are mainly from the interferences between the PGB amplitudes and the SM amplitude. In the case of $m_{\Pi_t^0} = 400$ GeV, $\Delta\sigma$ becomes positive. This is because the absolute squares of the Π_t and Π^0 resonance amplitudes are large in this case due to the enhancement of the photon spectral luminosity in the region around 400 GeV (80% of the e^+e^- energy) in the case of $2\lambda_e P_c = -1$ at the polarized photon collider [9].

TABLE II. Technipion and top-pion corrections to the $\gamma\gamma \to t\bar{t}$ cross section $\Delta\sigma$, the relative correction $\Delta\sigma/\sigma_0$, the total cross section $\sigma = \sigma_0 + \Delta\sigma$, and N_{events} for an integrated luminosity of 500 fb^{-1} taking account of the 10% detection efficiency at a 500 GeV e^+e^- linear colliderfor with $2\lambda_e P_c = -1$ for $m_t' = 14$ GeV, $m_{\Pi^3} = 300$ GeV, and various values of $m_{\Pi_t^0}$ and m_{Π^0} in model B (the SM cross section is $\sigma_0 = 196$ fb).

$m_{\Pi_t} = 300$ GeV				
m_{Π^0}	$\Delta\sigma$ (fb)	$\Delta\sigma/\sigma_0$ (%)	σ (fb)	N_{events}
300	−86.2	−44.0	110	5500
400	−47.2	−24.1	149	7450
500	−87.4	−44.6	109	5450
$m_{\Pi_t} = 400$ GeV				
m_{Π^0}	$\Delta\sigma$ (fb)	$\Delta\sigma/\sigma_0$ (%)	σ (fb)	N_{events}
300	112	57.1	308	15 400
400	158.3	80.8	354	17 700
500	115	58.7	311	15 550

To have an insight of the detailed situation, we plot the $t\bar{t}$ invariant mass distributions in Figs. 1 and 2 for the six sets of parameters in Table II. Figure 1 shows the invariant mass distributions for $m_{\Pi_t} = 300$ GeV, $m_\Pi = 300$, 400, and

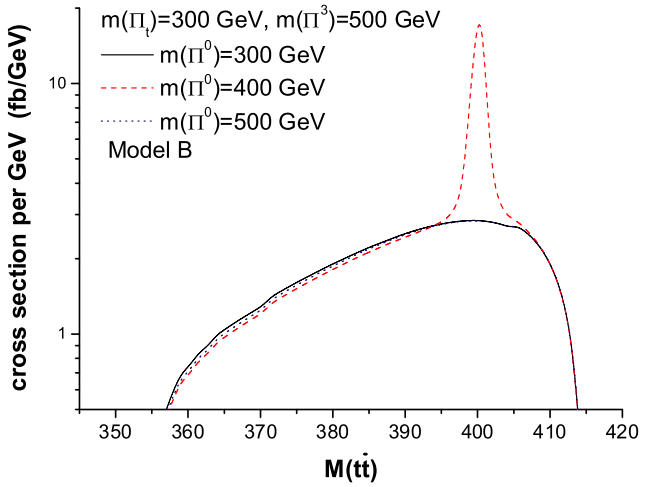

FIG. 1 (color online). $t\bar{t}$ invariant mass distribution in model B for $m_{\Pi_t} = 300$ GeV and $m_\Pi = 300$, 400, and 500 GeV.

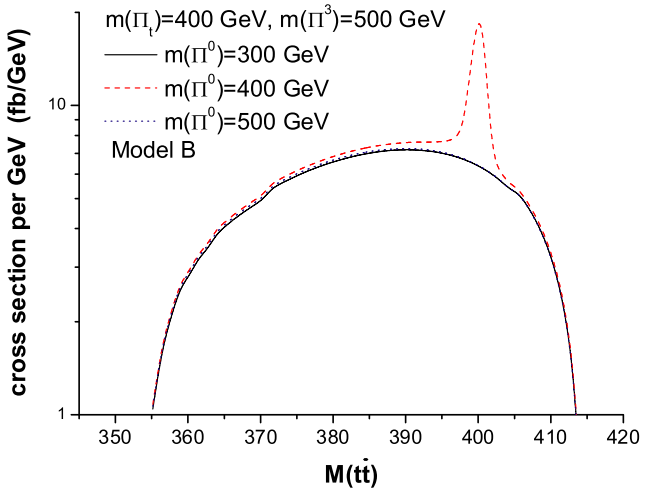

FIG. 2 (color online). $t\bar{t}$ invariant mass distribution in model B for $m_{\Pi_t} = 400$ GeV and $m_{\Pi} = 300$, 400, and 500 GeV.

TABLE III. Technipion and top-pion corrections to the $\gamma\gamma \to t\bar{t}$ cross section $\Delta\sigma$, the relative correction $\Delta\sigma/\sigma_0$, the total cross section $\sigma = \sigma_0 + \Delta\sigma$, and N_{events} for an integrated luminosity of 500 fb^{-1} taking account of the 10% detection efficiency at a 500 GeV e^+e^- linear colliderfor with $2\lambda_e P_c = -1$ for $m_t' = 14$ GeV and various values of m_{Π_t} and m_{Π^0} in model C with $m_{\Pi^3} = 300$ GeV (the SM cross section is $\sigma_0 = 196$ fb).

$m_{\Pi_t} = 300$ GeV				
m_{Π^0}	$\Delta\sigma$ (fb)	$\Delta\sigma/\sigma_0$ (%)	σ (fb)	N_{events}
300	−22.1	−11.3	174	8 700
400	469.2	239.4	665	33 250
500	−92.3	−47.1	104	5 200
$m_{\Pi_t} = 400$ GeV				
m_{Π^0}	$\Delta\sigma$ (fb)	$\Delta\sigma/\sigma_0$ (fb)	σ (fb)	N_{events}
300	79.1	40.4	275	13 750
400	1647.3	840.5	1843	92 150
500	125.7	64.1	322	16 100

500 GeV. We see that all curves are enhanced in the region around 400 GeV which is just the effect of the photon spectral luminosity. In the $m_{\Pi^0} = 400$ GeV distribution, we see a clear peak at 400 GeV. In the $m_{\Pi^0} = 300$ and 500 GeV distributions no clear peaks can be seen. This is because the probability of the center-of-mass energy of the two colliding photons being 300 or 500 GeV is very small as can be seen from the photon spectral luminosity [9]. We cannot see the top-pion resonance since the width of the top pion is much larger. Figure 2 shows the invariant mass distributions for $m_{\Pi_t} = 400$ GeV. The behaviors are similar but the enhancement around 400 GeV is stronger due to the s-channel contribution of the $m_{\Pi_t} = 400$ GeV top pion.

In the case of $m_{\Pi_t} = 300$ GeV, N_{events} is (5.4–7.5) × 10^3 (cf. Table II). The 95% C.L. statistical uncertainties are thus (2–3)%. Comparing with the relative corrections $\Delta\sigma/\sigma_0 = (24–45)\%$ in Table II, we see that these correction effects can be very clearly detected. For distinguishing model B from model A, we see that the relative difference between the total cross sections in models A and B is $[\sigma(A) - \sigma(B)]/\sigma(A) = (15–40)\%$, so that these two models can be very clearly distinguished.

In the case of $m_{\Pi_t} = 400$ GeV, N_{events} is (1.5–1.7) × 10^4. The corresponding 95% C.L. statistical uncertainties are (1.5–1.6)%. Now the relative corrections are $\Delta\sigma/\sigma_0 = (57–81)\%$ in Table II, so that these correction effects can be very clearly detected. The relative difference between the total cross sections in models A and B is now $[\sigma(A) - \sigma(B)]/\sigma(A) = -(71–100)\%$, thus these two models can be very clearly distinguished.

Model C.—Model C is similar to model B, but the decay constant of the color-singlet technipions is $f_\Pi = 40$ GeV rather than $f_\Pi \approx 120$ GeV [4]. Moreover, the coupling constant c_t in Eq. (11) and the Π^0-γ-γ coupling are also different from those in model B [4,7]. The smallness of f_Π makes the coupling constants m_t'/f_Π in Eqs. (10) and (11) larger than those in model B by a factor of 3. These changes enhance the s-channel Π^0 resonance effect in model C significantly. Furthermore, the 2σ R_b bound on the top-pion mass in this model is roughly $250 \leq m_{\Pi_t} \leq 560$ GeV [8]. To compare with model B, we also take the range $300 \leq m_{\Pi_t} \leq 500$ GeV in this study.

As in the case of model B, we examine the cases of $m_{\Pi_t} = 300$ and 400 GeV, and $m_{\Pi^0} = 300$, 400, and 500 GeV, with a typical value of the Π^3 mass, $m_{\Pi^3} = 300$ GeV. The obtained values of $\Delta\sigma$, $\Delta\sigma/\sigma_0$, and σ are listed in Table III. We see that $\Delta\sigma$ is negative only in the case of $m_{\Pi_t} = m_{\Pi^0} = 300$ GeV. In all other cases, $\Delta\sigma$ is positive because the absolute square of the Π^0 resonance amplitude is large due to the largeness of the coupling constant m_t'/f_Π. This effect is very significant in the case of $m_{\Pi_t} = m_{\Pi^0} = 400$ GeV.

In Figs. 3 and 4, we plot the $t\bar{t}$ invariant mass distributions in model C for $m_{\Pi_t} = 300$ and 400 GeV and $m_{\Pi^0} = 300$, 400, and 500 GeV. Again, we see the clear Π^0 resonance peak at 400 GeV, but the width of the resonance is much larger than that in Figs. 1 and 2 due to the largeness of the $\Pi^0 \to$ gluons and $\Pi^0 \to t\bar{t}$ widths.

In the case of $m_{\Pi_t} = 300$ GeV, N_{events} is (5.2–33) × 10^3. The corresponding 95% C.L. statistical uncertainties are then (1–3)%. Compared with the large relative corrections $\Delta\sigma/\sigma_0$ listed in Table III, we see that the PGB effects in model C can be clearly detected. Comparing the relative corrections $\Delta\sigma/\sigma_0$ listed in Table III and Table II, we see that the difference between model C and model B is significant for $m_{\Pi^0} = 300$ and 400 GeV. For $m_{\Pi^0} = 500$ GeV, the relative difference is $[\sigma(B) = \sigma(C)]/\sigma(B) = [109 - 104]/109 = 5\%$ which is also be-

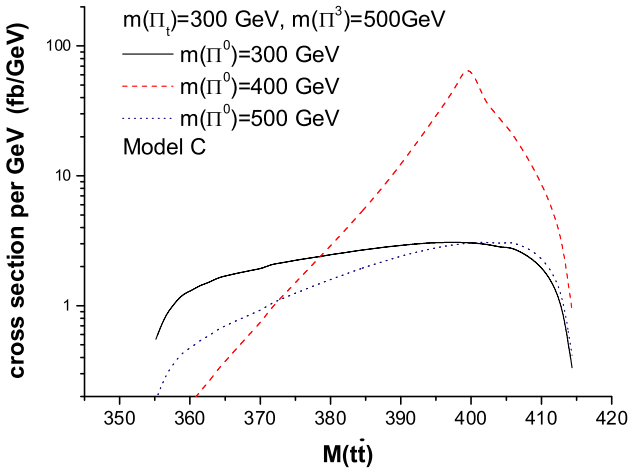

FIG. 3 (color online). $t\bar{t}$ invariant mass distribution in model C for $m_{\Pi_t} = 300$ GeV and $m_{\Pi} = 300$, 400, and 500 GeV.

yond the statistical uncertainties. Thus models C and B can be clearly distinguished from the production cross sections.

We see from Table III and Table I that, for most values of the PGB masses, model C can be distinguished from model A. The only case which needs to be studied more carefully is distinguishing the cases of model C with $m_{\Pi_t} = m_{\Pi^0} = 300$ GeV from model A with $m_{\Pi_a} =$ 350–400 GeV. From Table III and Table I, we see that the total cross sections for these two cases are almost the same, so that they cannot be distinguished by merely measuring the total cross sections. Since the numbers of events are around 8700–8850, it is possible to measure the $t\bar{t}$ invariant mass ($M_{t\bar{t}}$) distribution. In Fig. 5 we plot the $M_{t\bar{t}}$ distributions for the two cases.

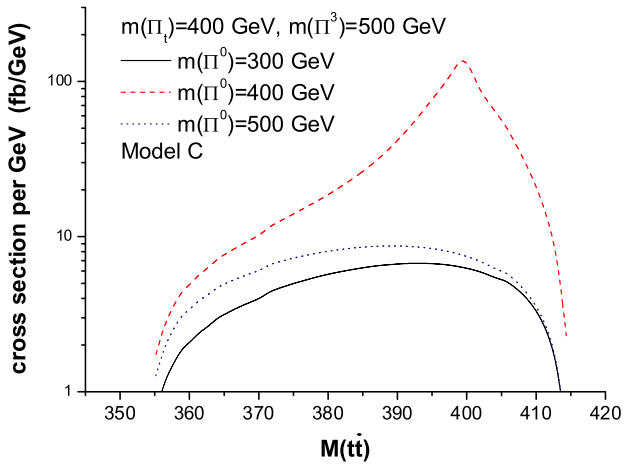

FIG. 4 (color online). $t\bar{t}$ invariant mass distribution in model C for $m_{\Pi_t} = 400$ GeV and $m_{\Pi} = 300$, 400, and 500 GeV.

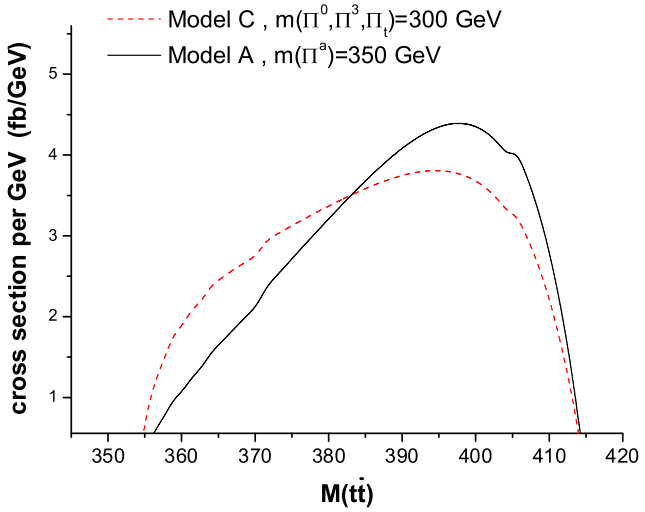

FIG. 5 (color online). Comparison of the $t\bar{t}$ invariant mass distributions in model C for $m_{\Pi_t} = m_{\Pi} = m_{\Pi_a} = 300$ GeV and model A for $m_{\Pi_a} = 350$ GeV.

To make it more realistic, we should further take into account the effect of energy resolution. According to Ref. [16], the energy resolution is $\Delta E/E = 0.33/\sqrt{E}$. We then smear the calculated $M_{t\bar{t}}$ by taking convolutions with this resolution. The obtained smeared $M_{t\bar{t}}$ distributions for the above two cases are shown in Fig. 6. We see that they are different, especially in the vicinities of 365 and 400 GeV where the differences are of the level of (10–40)%. According to the energy resolution, the resolution

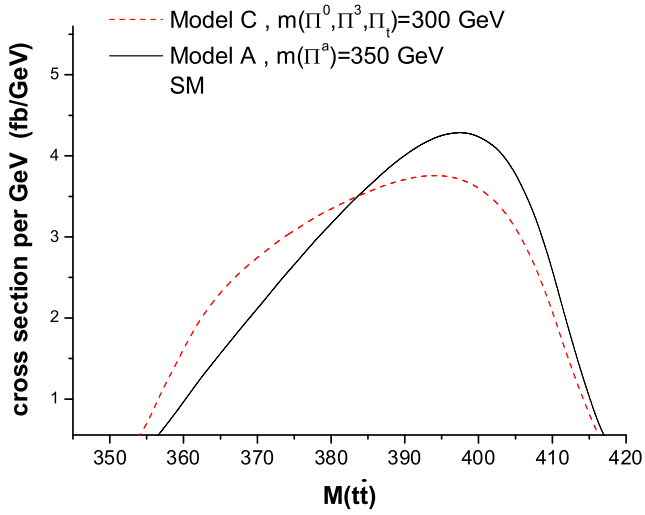

FIG. 6 (color online). Comparison of the smeared $t\bar{t}$ invariant mass distributions in model C for $m_{\Pi_t} = m_{\Pi} = m_{\Pi_a} =$ 300 GeV and model A for $m_{\Pi_a} = 350$ GeV according to the resolution $\Delta E/E = 0.33/\sqrt{E}$.

for measuring the $M_{t\bar{t}}$ distribution around 400 GeV is $\Delta M_{t\bar{t}} = 0.33 \times \sqrt{400}\ \text{GeV} = 6.6\ \text{GeV}$, so that the above two cases in models A and C can be distinguished by separately measuring the numbers of events in the regions $355 \leq M_{t\bar{t}} \leq 375$ GeV and $390 \leq M_{t\bar{t}} \leq 410$ GeV.

In the case of $m_{\Pi_t} = 400$ GeV, we can see that model C is very different from the SM, and all three models can be distinguished.

In summary, we have studied the possibility of testing and distinguishing three improved technicolor models (models A, B, and C) via $t\bar{t}$ productions at a polarized photon collider with $2\lambda_e P_c = -1$ from a 500 GeV e^+e^- linear collider with an integrated luminosity of 500 fb^{-1}. The signal contains six jets from $t \to W^+ b$ and $W \to q\bar{q}'$. Backgrounds can be suppressed by taking the cut (6) and tagging a b quark jet. Considering the possible detection ability of the detector and the usual b-tagging efficiency, the detection efficiency is 10%. We see that, considering only the statistical error, the three improved technicolor models can all be well tested and can be distinguished from each other by measuring the $\gamma\gamma \to t\bar{t}$ production cross section and the $t\bar{t}$ invariant mass distribution.

We would like to thank C.-P. Yuan for discussions. This work is supported by the National Natural Science Foundation of China under Grant No. 90103008.

[1] Particle Data Group, S. Eidelman *et al.*, Phys. Lett. B **592**, 1 (2004).
[2] T. Appelquist and J. Terning, Phys. Lett. B **315**, 139 (1993).
[3] C. T. Hill, Phys. Lett. B **345**, 483 (1995); K. Lane and E. Eichten, *ibid.* **352**, 382 (1995); G. Buchalla, G. Burdan, C. T. Hill, and D. Kominis, Phys. Rev. D **53**, 5185 (1996).
[4] K. Lane, Phys. Lett. B **357**, 624 (1995).
[5] B. A. Dobrescu and C. T. Hill, Phys. Rev. Lett. **81**, 2634 (1998); R. S. Chivukula, B. A. Dobrescu, H. Georgi, and C. T. Hill, Phys. Rev. D **59**, 075003 (1999); H.-J. He, C. T. Hill, and T. Tait, Phys. Rev. D **65**, 055006 (2002).
[6] N. Arkani-Hammed, A. G. Cohen, and H. Georgi, Phys. Lett. B **513**, 232 (2001); N. Arkani-Hammed, A. G. Chen, E. Katz, A. E. Nelson, T. Gregoire, and J. G. Wacker, J. High Energy Phys. 08 (2002) 021; J. G. Wacker, hep-ph/0208235; N. Arkani-Hammed, A. G. Cohen, E. Katz, and A. E. Nelson, J. High Energy Phys. 07 (2002) 034; T. Gregoire and J. G. Wacker, hep-ph/0207164; I. Low, W. Skiba, and D. Smith, Phys. Rev. D **66**, 072001 (2002).
[7] H.-Y. Zhou, Y.-P. Kuang, C.-X. Yue, H. Wang, and G.-R. Lu, Phys. Rev. D **57**, 4205 (1998).
[8] C.-X. Yue, Y.-P. Kuang, X.-L. Wang, and W. B. Li, Phys. Rev. D **62**, 055005 (2000).
[9] I. F. Ginzburg, G. L. Kotkin, S. L. Panfil, V. G. Serbo, and V. I. Telnov, Nucl. Instrum. Methods Phys. Res. **219**, 5 (1984); B. Badelek *et al.*, DESY Report No. 2001-011, 2001, Part VI of TESLA Technical Design Report.
[10] O. J. P. Eboli *et al.*, Phys. Rev. D **47**, 1889 (1993); K. Cheung, *ibid.* **47**, 3750 (1993).
[11] V. M. Budnev, I. F. Ginzburg, G. V. Meledin, and V. G. Serbo, Phys. Rep. C **15**, 181 (1975).
[12] KEK Report No. 2001-11, 2001 (JLC Technical Design Report).
[13] M. Baillargeon *et al.*, DESY Report No. 96-123D, 1995, edited by P. Zerwas; see also DESY Report No. 2001-011, 2001, Part VI of TESLA Technical Design Report No.
[14] DESY Report No. 2001-011, 2001, Part I of TESLA Technical Design Report.
[15] B. Balaji, Phys. Rev. D **53**, 1699 (1996).
[16] DESY Report No. 2001-011, 2001, Part IV of TESLA Technical Design Report.